

# Revisiting general dark matter-bound-electron interactions

Jin-Han Liang,<sup>1,2,\*</sup> Yi Liao,<sup>1,2,†</sup> Xiao-Dong Ma,<sup>1,2,‡</sup> and Hao-Lin Wang<sup>1,2,§</sup>

<sup>1</sup>Key Laboratory of Atomic and Subatomic Structure and Quantum Control (MOE),  
Guangdong Basic Research Center of Excellence for Structure and Fundamental Interactions of Matter,  
Institute of Quantum Matter, South China Normal University, Guangzhou 510006, China

<sup>2</sup>Guangdong-Hong Kong Joint Laboratory of Quantum Matter,  
Guangdong Provincial Key Laboratory of Nuclear Science, Southern Nuclear Science Computing Center,  
South China Normal University, Guangzhou 510006, China

In this letter we revisit general dark matter (DM)-bound-electron interactions studied previously in the influential work of [Catena *et al.*, *Phys. Rev. Res.* **2**, 033195 (2020)]. We derive the DM-electron response functions and find a crucial minus sign was missed for the second atomic response function  $W_2$  defined in that work. The minus sign has significant phenomenological consequences when explaining experimental bounds on specific DM scenarios. Furthermore, for the most general DM-electron nonrelativistic or relativistic interactions for DM with spin up to one, we find there are three DM response functions ( $a_{0,1,2}$ ) whose corresponding atomic response functions ( $\widetilde{W}_{0,1,2}$ ) are linear combinations of the four response functions ( $W_{1,2,3,4}$ ) given in that work,

$$\widetilde{W}_0 = W_1, \quad \widetilde{W}_2 = |\mathbf{v}_0^\perp|^2 W_1 + W_3 - 2 \frac{m_e \mathbf{q} \cdot \mathbf{v}_0^\perp}{q^2} W_2, \quad \widetilde{W}_3 = \frac{(\mathbf{q} \cdot \mathbf{v}_0^\perp)^2}{q^2} W_1 + \frac{m_e^2}{q^2} W_4 - 2 \frac{m_e \mathbf{q} \cdot \mathbf{v}_0^\perp}{q^2} W_2.$$

Due to the minus sign correction for  $W_2$ , there can be significant cancellations between the  $W_2$  and  $W_{3,4}$  terms, so that  $\widetilde{W}_{2,3}$  are dominated by the usual response function  $W_1$  in some cases. Ignoring the sign could thus result in misinterpretation of the experimental data in some DM scenarios. As an example, we show that the recent XENON1T constraint on the fermionic DM anapole moment is weakened by a factor of 2 or so. Many DM scenarios involving DM or electron axial-vector current can yield  $W_2$  and thus are potentially affected by the sign.

*Introduction.*—The nature of dark matter (DM) is one of the biggest puzzles in particle astrophysics. Particle DM is a well-motivated scenario that fits very well within the standard cosmological model ( $\Lambda$ CDM), and in the meanwhile has a detectable possibility in terrestrial experiments. The mass scale for potential DM candidates spans a very wide range of energy scales, from the superlight axion or dark photon candidate [1–3], to the keV sterile neutrino [4, 5], to relatively more massive particles that are generally termed weakly interacting massive particles (WIMPs) [6, 7]. Among them, the WIMPs are the most prominent ones in consideration of their origin in particle physics models, the power of fitting the observational data, and the promising discovery potential in direct detection experiments.

The search for WIMP DM begins with the nuclear recoil effect. The null results from large xenon and argon detectors (such as PandaX [8], XENON [9], LUX-ZEPLIN (LZ) [10], and DarkSide [11]) in the past two decades have put stringent bounds on the DM-nucleus cross section with DM mass above  $\mathcal{O}(10 \text{ GeV})$  [7, 12]. Due to the kinematic restriction of DM-nucleus (or DM-nucleon) elastic scattering as well as detection threshold limitation, the DM-nucleon interaction remains less constrained for DM mass below  $\mathcal{O}(10 \text{ GeV})$  from nuclear recoil signals. This limitation could be circumvented by exploiting inelastic processes like the bremsstrahlung process [13] and the Migdal effect [14, 15], or novel low-threshold detectors in condensed matter systems (see [16, 17] and references cited therein). In contrast to nu-

clear recoil experiments searching for the DM-nucleon interaction, the DM-electron interaction offers a more powerful alternative probe of low mass DM particles below  $\mathcal{O}(10 \text{ GeV})$  through the electron recoil signal [18–24]. This is due to the significantly smaller mass of the target electron, allowing it to gain more easily the recoil energy from a light DM particle. For instance, the single-electron search conducted by XENON1T has the capability of exploring DM as light as approximately 5 MeV [20].

Since the search for light DM through DM-electron scattering has become more and more important than ever before, a thorough understanding of the response functions of the electron in a target material is urgent. The dual-phase detectors, with liquid xenon or argon as the target material, are the most promising DM direct detection experiments to explore the parameter space of WIMPs in a wide mass region, and can effectively distinguish between the signals induced by the DM-electron and DM-nucleus scattering. Theoretically, the DM-electron scattering in a liquid xenon target was first calculated in [25–27], in which some simplified DM models were studied, with the atomic effect of bound electrons being encoded in the ionization form factor [26] or the  $K$ -factor [28]. The relativistic correction and many-body effect of the ionization form factor were further considered in [28–30], which could be sizable for a large transfer momentum. Recently, a general study on the atomic response functions in the liquid xenon and argon targets was carried out in [31] in the framework of nonrelativis-

tic (NR) effective field theory (EFT), in which three new atomic response functions were introduced in addition to the usual ionization form factor. These new atomic response functions appear for general DM-electron interactions and are particularly relevant for some special DM scenarios. They have been used in subsequent theoretical [32] and experimental [20] papers. In this work, we re-derive these response functions, and find that a crucial minus sign was missed for the second response function  $W_2$  defined in [31]. The minus sign is physically important when explaining experimental bounds in terms of specific DM scenarios. For the purpose of illustration and the interest in its own right, we study the constraints on the DM anapole operator which were considered previously in [20, 32]. We find that the constraints are weakened by a factor of 2 or so upon correcting the sign of  $W_2$ . Along the line we formulate the squared matrix element of the DM-atom scattering from the most general NR EFT operators for DM up to spin one, and find that it can be compactly organized into three terms (see Eq. (7)), each of which is a product of a DM response function and an atomic response function.

*Formalism for DM-atom scattering.*—For the DM-electron scattering in atomic target, we label the initial state of the bound electron by the usual atomic quantum numbers  $(n, \ell, m) \equiv |1\rangle$  and the final state of the ionized electron by  $(k', \ell', m') \equiv |2\rangle$  with  $k'$  being its momentum. Denoting the initial (final) momentum of DM by  $p$  ( $p'$ ), the transition amplitude for  $|p, 1\rangle \rightarrow |p', 2\rangle$  can be written as [31]

$$\mathcal{M}_{1\rightarrow 2} = \int \frac{d^3\mathbf{k}}{(2\pi)^3} \tilde{\psi}_2^*(\mathbf{k} + \mathbf{q}) \mathcal{M}(\mathbf{q}, \mathbf{v}_{\text{el}}^\perp) \tilde{\psi}_1(\mathbf{k}), \quad (1)$$

where  $\tilde{\psi}_1 \equiv \tilde{\psi}_{n\ell m}$  and  $\tilde{\psi}_2 \equiv \tilde{\psi}_{k'\ell'm'}$  are the initial and final electron wavefunctions in momentum space respectively, and are related to the wavefunctions in configuration space by the Fourier transformation,  $\tilde{\psi}(\mathbf{k}) = \int d^3\mathbf{r} e^{-i\mathbf{k}\cdot\mathbf{r}} \psi(\mathbf{r})$ .  $\mathcal{M}(\mathbf{q}, \mathbf{v}_{\text{el}}^\perp)$  is the matrix element for free electron-DM scattering that is only a function of the momentum transfer  $\mathbf{q} \equiv \mathbf{p} - \mathbf{p}'$  and the DM-electron transverse velocity  $\mathbf{v}_{\text{el}}^\perp = \mathbf{v} - \mathbf{q}/(2\mu_{xe}) - \mathbf{k}/m_e$  in the nonrelativistic framework. Here  $\mathbf{v}$  is the incoming DM velocity in the lab frame,  $\mathbf{k}$  is the momentum of the initial electron of mass  $m_e$ , and  $\mu_{xe}$  the reduced DM-electron mass, respectively.

For the most general DM-electron interactions at leading order in the NR EFT framework given in Table I in Appendix, which are at most linear order in  $\mathbf{v}_{\text{el}}^\perp$  or  $\mathbf{k}$ , the free amplitude is decomposed as [31],  $\mathcal{M} = \mathcal{M}_{\mathbf{k}=0} + \mathbf{k} \cdot (\nabla_{\mathbf{k}} \mathcal{M})_{\mathbf{k}=0}$ . This results in two atomic form factors  $f_{1\rightarrow 2}(\mathbf{q})$  and  $\mathbf{f}_{1\rightarrow 2}(\mathbf{q})$  in Eq. (1):

$$f_{1\rightarrow 2}(\mathbf{q}) = \int \frac{d^3\mathbf{k}}{(2\pi)^3} \tilde{\psi}_2^*(\mathbf{k} + \mathbf{q}) \tilde{\psi}_1(\mathbf{k}), \quad (2a)$$

$$\mathbf{f}_{1\rightarrow 2}(\mathbf{q}) = \int \frac{d^3\mathbf{k}}{(2\pi)^3} \tilde{\psi}_2^*(\mathbf{k} + \mathbf{q}) \frac{\mathbf{k}}{m_e} \tilde{\psi}_1(\mathbf{k}). \quad (2b)$$

The first one is the usual ionization form factor, while the second was first recognized in [31]. We find that a minus sign was missed in the vector form factor  $\mathbf{f}_{1\rightarrow 2}(\mathbf{q})$  of [31] when transforming from momentum to configuration space,

$$f_{1\rightarrow 2}(\mathbf{q}) = \int d^3\mathbf{r} \psi_2^*(\mathbf{r}) e^{i\mathbf{q}\cdot\mathbf{r}} \psi_1(\mathbf{r}), \quad (3a)$$

$$\mathbf{f}_{1\rightarrow 2}(\mathbf{q}) = \int d^3\mathbf{r} \psi_2^*(\mathbf{r}) e^{i\mathbf{q}\cdot\mathbf{r}} \frac{-i\nabla}{m_e} \psi_1(\mathbf{r}). \quad (3b)$$

This will cause a considerable impact on the matrix element squared as spelled out below.

The decomposition of  $\mathcal{M}$  in terms of  $\mathbf{k}$  leads the authors in [31] to identify three additional atomic response functions  $W_{2,3,4}$  beyond the usual  $W_1$ . From their definitions reproduced in Appendix, one sees that the minus sign in  $\mathbf{f}_{1\rightarrow 2}(\mathbf{q})$  is brought into the function  $W_2$ . To appreciate the consequence of this sign, we decompose the free matrix element into the  $\mathbf{v}_{\text{el}}^\perp$  independent and linearly-dependent parts as suggested by the defining form of NR operators,

$$\begin{aligned} \mathcal{M}(\mathbf{q}, \mathbf{v}_{\text{el}}^\perp) &= \mathcal{M}(\mathbf{q}, 0) + \mathbf{v}_{\text{el}}^\perp \cdot \nabla_{\mathbf{v}_{\text{el}}^\perp} \mathcal{M}(\mathbf{q}, \mathbf{v}_{\text{el}}^\perp) \\ &= \mathcal{M}_{\text{S}} + \left( \mathbf{v}_0^\perp - \frac{\mathbf{k}}{m_e} \right) \cdot \mathcal{M}_{\text{V}}, \end{aligned} \quad (4)$$

where  $\mathcal{M}_{\text{S}} \equiv \mathcal{M}(\mathbf{q}, 0)$ ,  $\mathcal{M}_{\text{V}} \equiv \nabla_{\mathbf{v}_{\text{el}}^\perp} \mathcal{M}(\mathbf{q}, \mathbf{v}_{\text{el}}^\perp)$ , and the  $\mathbf{k}$ -independent part of  $\mathbf{v}_{\text{el}}^\perp$  is denoted by  $\mathbf{v}_0^\perp \equiv \mathbf{v} - \mathbf{q}/(2\mu_{xe})$ . We find the spin-averaged atomic matrix element squared takes the form,

$$\begin{aligned} |\overline{\mathcal{M}_{1\rightarrow 2}}|^2 &= a_0 |f_{\text{S}}|^2 + a_1 |\mathbf{f}_{\text{V}}|^2 + \frac{a_2}{x_e} \left| \frac{\mathbf{q}}{m_e} \cdot \mathbf{f}_{\text{V}} \right|^2 \\ &\quad + i a_3 \frac{\mathbf{q}}{m_e} \cdot (\mathbf{f}_{\text{V}} \times \mathbf{f}_{\text{V}}^*) + 2 \text{Im} \left[ a_4 f_{\text{S}} \mathbf{f}_{\text{V}}^* \cdot \frac{\mathbf{q}}{m_e} \right], \end{aligned} \quad (5)$$

where  $x_e \equiv \mathbf{q}^2/m_e^2$  and  $y_e \equiv \mathbf{q} \cdot \mathbf{v}_0^\perp/m_e$ ,  $f_{\text{S}}(\mathbf{q}) \equiv f_{1\rightarrow 2}(\mathbf{q})$ , and  $\mathbf{f}_{\text{V}}(\mathbf{q}) \equiv \mathbf{v}_0^\perp f_{1\rightarrow 2}(\mathbf{q}) - \mathbf{f}_{1\rightarrow 2}(\mathbf{q})$ .  $a_{0,1,2,3,4}$  are DM response functions depending only on the Wilson coefficients (WCs) of NR operators and  $x_e$ . The explicit forms of  $a_{0,1,2}$  are provided in Eq. (12), Eq. (13), and Eq. (14) for the scalar, fermion, and vector DM cases in Appendix, respectively. The other two terms  $a_{3,4}$  have no contribution to the usual DM-atom scattering after summing over the atomic magnetic quantum numbers  $(m, m')$ , and will be presented in the accompanying long paper [33].

With  $|\overline{\mathcal{M}_{1\rightarrow 2}}|^2$  in Eq. (5), the total ionization rate for the initial atomic orbital  $(n, \ell)$ ,  $\mathcal{R}_{\text{ion}}^{n\ell}$ , can be obtained by summing over the initial magnetic quantum number  $m$  and integrate/sum over all the allowed final electron states  $(k', \ell', m')$ . Neglecting the effect arising from the non-spherically symmetric nature of the DM velocity distribution in the lab frame, the differential rate can be

generally written as [31, 34]

$$\frac{d\mathcal{R}_{\text{ion}}^{n\ell}}{d\ln E_e} = \frac{n_{\text{dm}}}{128\pi^2 m_{\text{dm}}^2 m_e^2} \int dq q \int \frac{d^3\mathbf{v}}{v} f_{\text{dm}}(\mathbf{v}) \overline{|\mathcal{M}_{\text{ion}}^{n\ell}|^2}, \quad (6)$$

where  $n_{\text{dm}}$  is the local DM number density with velocity distribution  $f_{\text{dm}}(\mathbf{v})$  and  $m_{\text{dm}}$  is the DM mass. The integration over  $v$  is bounded below by  $v_{\text{min}}$  due to the kinematics restriction. Using the decomposition in Eq. (4) and the squared matrix element in Eq. (5), our main result in this letter is the recognition of the averaged ionization matrix element squared,

$$\overline{|\mathcal{M}_{\text{ion}}^{n\ell}|^2} = a_0 \widetilde{W}_0 + a_1 \widetilde{W}_1 + a_2 \widetilde{W}_2, \quad (7)$$

where the atomic response functions  $\widetilde{W}_{0,1,2}$  are related to  $W_{1,2,3,4}$  in [31] as,<sup>1</sup>

$$\widetilde{W}_0 = W_1, \quad (8a)$$

$$\widetilde{W}_1 = |\mathbf{v}_0^\perp|^2 W_1 - 2 \frac{y_e}{x_e} W_2 + W_3, \quad (8b)$$

$$\widetilde{W}_2 = \frac{y_e^2}{x_e} W_1 - 2 \frac{y_e}{x_e} W_2 + \frac{1}{x_e} W_4. \quad (8c)$$

We find the decomposition in Eq. (4) is more amenable to obtain the square of the ionization matrix element with  $a_0$  and  $a_{1,2}$  capturing different NR contributions, as can be seen explicitly from Eq. (12), Eq. (13), and Eq. (14) in Appendix. Furthermore, the recognition of the three new combinations of atomic response functions is useful to understand which NR operators contribute dominantly to the scattering. In Eq. (7),  $\widetilde{W}_0$  (or  $W_1$ ) is the usual atomic  $K$ -factor in the literature [28, 35]. Its associated DM response function  $a_0$  incorporates the most common DM scenarios through the WCs  $c_1$  and  $c_4$  of the NR operators  $\mathcal{O}_1$  and  $\mathcal{O}_4$ , which are the well-known spin-independent and spin-dependent NR interactions extensively studied in the literature.  $\widetilde{W}_{1,2}$  are mainly related to the NR operators involving transverse velocity  $\mathbf{v}_{\text{el}}^\perp$ , which can be generated by DM-electron interactions involving electron or DM axial-vector current such as the anapole moment of fermionic DM. Thus, a sign mistake in  $W_2$  will result in a wrong interpretation of experimental data for such types of interactions.

To assess the numerical importance of the sign, we show in Fig. 1 the individual terms of  $\widetilde{W}_{1,2}$  as a function of the momentum transfer  $|\mathbf{q}|$  for a xenon target in the orbital 5p. We choose a typical light DM mass  $m_{\text{dm}} = 500$  MeV and fix the ionized electron momentum to be  $k' = 10$  keV. From Fig. 1, it is clear that the  $W_2$

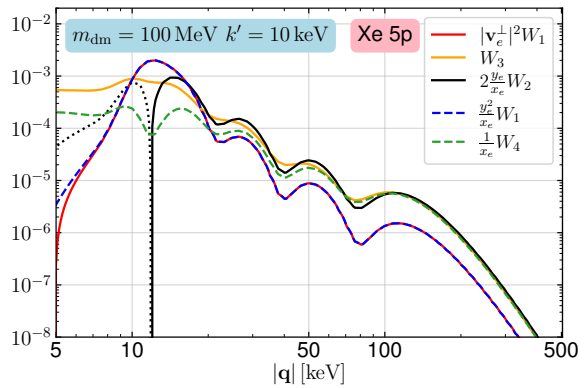


FIG. 1: Individual terms in  $\widetilde{W}_{1,2}$  are shown as a function of  $|\mathbf{q}|$ . For better layout we show  $-2(y_e/x_e)W_2$  (black dotted curve) for  $|\mathbf{q}| \lesssim 11.5$  keV and  $+2(y_e/x_e)W_2$  (black solid) for  $|\mathbf{q}| \gtrsim 11.5$  keV. The lower limit of  $|\mathbf{q}|$  is determined by kinematic consideration.

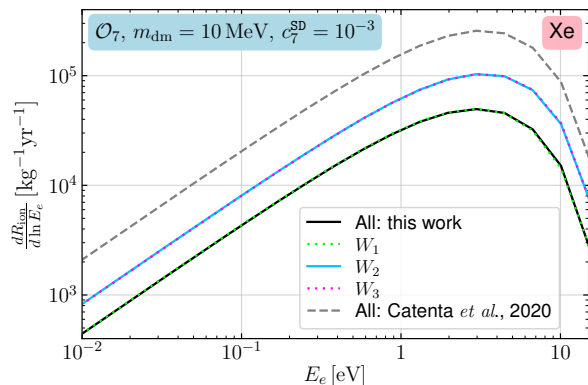


FIG. 2: The ionization spectrum from the NR interaction  $\mathcal{O}_7$  with a short distance origin at the xenon target from different response functions. The DM can be either a scalar, fermion, or vector particle. Note that the solid black and dotted green curves almost overlap.

term is positive for  $|\mathbf{q}| \gtrsim 11.5$  keV, and approaches  $W_3$  and  $W_4/x_e$  as  $|\mathbf{q}|$  increases. With the minus sign accompanying  $W_2$  in  $\widetilde{W}_{1,2}$ , it implies there is a significant cancellation between the  $W_2$  and  $W_{3,4}$  terms in  $\widetilde{W}_{1,2}$ , leaving the  $W_1$  term as the potentially dominant contribution across a wide region of  $|\mathbf{q}|$ . This behavior is common to other atomic orbitals, DM mass, and the ionized electron momentum.

Next we examine the influence on the differential rate due to the NR operator  $\mathcal{O}_7$ , which is a typical operator employed in [31] to show the importance of the three new response functions ( $W_2, W_3, W_4$ ). To facilitate comparison with [31], we consider the xenon and argon targets and focus on the contact (or short-distance) interaction

<sup>1</sup> Notice that both  $\widetilde{W}_i$  and  $W_i$  depend on the initial atomic quantum numbers ( $n, \ell$ ), the final electron momentum  $k'$ , and the momentum transfer  $|\mathbf{q}|$ . We do not show them explicitly for brevity.

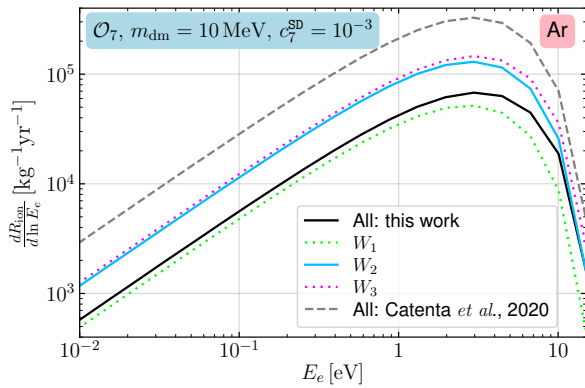


FIG. 3: Same as Fig. 2 except for an argon target.

with  $c_{10}^{\text{SD}} = 10^{-3}$  and  $m_{\text{dm}} = 10 \text{ MeV}$ . In Fig. 2, we show for the xenon target the individual contribution to the differential rate from  $W_1$ ,  $W_2$ , and  $W_3$  (including all coefficients but not the minus sign in front of  $W_2$  in Eq. (8) for better layout) by the dotted green, solid blue, and dotted magenta curves. From Fig. 2, it can be seen that the contributions from  $W_2$  and  $W_3$  are of a similar magnitude and much larger than that from  $W_1$ , so that they almost exactly cancel out, leading to a total contribution (solid black curve) that is completely dominated by  $W_1$ . For comparison, we also show the total rate reported in [31] by the dashed black curve.<sup>2</sup> It can be seen that the sign difference can cause up to an order of magnitude difference in the differential rate. A similar plot for the argon target is provided in Fig. 3. In that case, the cancellation between  $W_2$  and  $W_3$  is less complete, leading to a slightly higher total contribution than that from  $W_1$  alone. Note that the spectrum is the same for  $\mathcal{O}_8$  with fermion DM as indicated in Eq. (13), which will be used in the following analysis.

*Constraints on DM anapole.*—In this part, we use the DM anapole operator as an example to illustrate the importance of the sign for  $W_2$ . The anapole interaction Lagrangian for a fermionic DM  $\chi$  is

$$\mathcal{L}_{\text{anapole}} = \frac{g}{2\Lambda^2} \bar{\chi} \gamma^\mu \gamma^5 \chi \partial^\nu F_{\mu\nu}, \quad (9)$$

where  $F_{\mu\nu}$  is the electromagnetic field strength tensor,  $g$  is a dimensionless coupling, and  $\Lambda$  is a heavy particle scale. We consider  $\chi$  as a Majorana particle for direct comparison with the results in the literature [20, 31]. The anapole moment is the unique electromagnetic property of a Majorana fermion since all others (such as charge

radius and electromagnetic dipole moments) do not exist. In the NR limit, the DM anapole operator matches to two NR operators,  $\mathcal{O}_8$  and  $\mathcal{O}_9$ , with the WCs,

$$c_8 = -c_9 = 8 e m_e m_\chi \frac{g}{\Lambda^2}. \quad (10)$$

Since the sign of  $W_2$  has a significant impact on the contribution from  $\mathcal{O}_8$ , as illustrated in Fig. 2, it is expected that it also plays a crucial role in determining the constraints on the DM anapole operator. The previous constraints were established using data from various experiments, including XENON10, DarkSide-50, the XENON1T S2-only search (calculated in [31]), and the XENON1T single electron (SE) search conducted by the XENON1T collaboration [20]. All of these constraints were obtained with a wrong sign associated with  $W_2$ . In the following, we analyze these constraints from xenon target experiments. In addition, we calculate the constraint using the latest S2-only data from the PandaX-4T experiment [22].

To compare with the S2-only data observed in the experiments, we utilize the constant-W model [27, 36] to convert the  $d\mathcal{R}_{\text{ion}}^{n\ell}/dE_e$  spectrum into that of the number of ionized electrons,  $d\mathcal{R}_{\text{ion}}^{n\ell}/dn_e$ . For each ionized electron, we assume that the number of photoelectrons (PEs) induced by it follows a Gaussian distribution with a mean value  $g_2$  and a width value  $\sigma_{S2}$  as in [27, 36]. Specifically, for XENON10 (XENON1T), we take  $g_2 = 27$  (33) and  $\sigma_{S2} = 6.7$  (7) [36, 37]. By convoluting with the Gaussian distribution [19, 27, 36], we obtain the spectrum of S2 signals (the number of PEs),  $d\mathcal{R}_{\text{ion}}^{n\ell}/d\text{PE}$ . For the constraints from the XENON10 and XENON1T S2-only searches, we employ the same efficiency factors and statistical methods as in [31]. With a wrong sign of  $W_2$  we were able to reproduce the constraints in [31] to check our numerical analysis.

**XENON1T-SE:** Since the XENON1T collaboration did not provide all the necessary information in their paper [20], it is challenging to reproduce its constraint with high consistency. Therefore, we adopt a rescaling method to be described below to update the constraint with the corrected sign of  $W_2$ . The signal region in the XENON1T SE search is selected as  $S2 \in [14, 150]$  PE, corresponding to signals with 1–5 ionized electrons [20]. For a specific DM mass, we find that the spectrum  $d\mathcal{R}_{\text{ion}}^{n\ell}/dn_e$  with the correct-sign  $W_2$  differs from that with the wrong-sign  $W_2$  by nearly a global factor. For instance, for  $m_\chi = 1 \text{ GeV}$ , this global factor is approximately 3 for the anapole operator. Hence, for each DM mass, we calculate  $\sum_{n_e=1}^5 d\mathcal{R}_{\text{ion}}^{n\ell}/dn_e$  with both the wrong-sign and correct-sign  $W_2$ . Then, we deliver our new constraint by rescaling the constraint of the XENON1T collaboration.

**PandaX-4T:** With the exposure of 0.55 ton-yr, 103 events (including 95.8 background events estimated) were observed in the signal region of  $S2 \in [60, 200]$  PE [22]. According to the Poisson distribution, a 90% C.L. requires

<sup>2</sup> There is about a global factor of 3/4 difference than the one given in [31], which has been included in our plot.



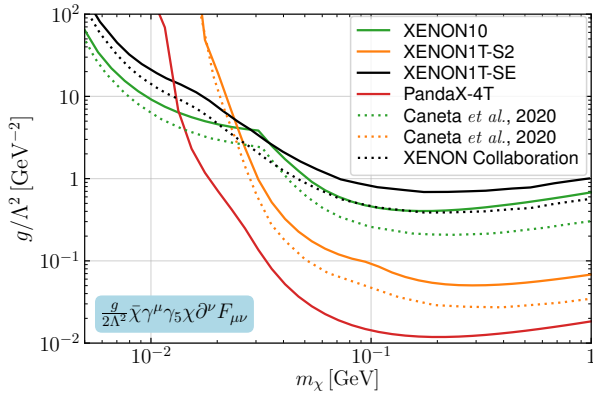


FIG. 4: Constraints on DM anapole moment from DM direct detection experiments, including XENON10, XENON1T S2-only search, XENON1T-SE search, and PandaX-4T. The solid lines show our results with a correct-sign  $W_2$ , while the dashed lines show the previous constraints [20, 31] with a wrong-sign  $W_2$ .

the number of signal events to be less than 21.5. We employ the total efficiency (red solid line) given in Fig. (1) of [22]. Since the parameters  $g_2$  and  $\sigma_{S2}$  of the PandaX-4T S2-only search were not given explicitly in the paper, we read from its Fig. (3)  $g_2 = 17.7$  and assume  $\sigma_{S2} = \sqrt{g_2}$ .

To ensure consistent comparison with previous calculations based on a wrong-sign  $W_2$ , we adopt the same DM parameters as [31]:  $\rho_\chi = 0.4 \text{ GeV/cm}^3$  for the local DM density,  $v_0 = 220 \text{ km/s}$  for the Sun’s circular velocity,  $v_{\text{esc}} = 544 \text{ km/s}$  for the galactic escape velocity, and  $v_\oplus = 244 \text{ km/s}$  for the speed of Earth in the galactic rest frame. Our results on XENON10, XENON1T S2, and XENON1T SE, and the latest PandaX-4T data are shown in Fig. 4 with solid curves. Correcting the  $W_2$  sign, the constraints are weakened by a factor of  $\sim 2$ , depending on the DM mass. With a larger DM mass, the discrepancy tends to be larger. The constraint derived from the latest PandaX-4T data imposes the most stringent limit for DM mass  $m_\chi \gtrsim 20 \text{ MeV}$ , reaching  $g/\Lambda^2 \lesssim 0.01 \text{ GeV}^{-2}$  for  $m_\chi \gtrsim 0.1 \text{ GeV}$ . In the low-mass region with  $m_\chi \lesssim 20 \text{ MeV}$ , the stronger limit is set by the previous XENON10 and XENON1T-SE experiments, which have a low energy threshold down to one single ionized electron.

*Conclusion.*—In this letter, we studied the general DM-electron interactions and found, for the most general leading-order nonrelativistic dark matter-electron interactions, that those interactions naturally organize themselves into the differential rate in the form of three DM response functions  $a_{0,1,2}$ . Each of  $a_{0,1,2}$  is multiplied by an atomic response function  $\widetilde{W}_{0,1,2}$  which is a linear combination of the four atomic response functions  $W_{1,2,3,4}$  defined in [31]. Most importantly, we found a crucial sign

mistake associated with  $W_2$ . Our results show that this leads to important phenomenological implications. As far as general NR operators are concerned, it will influence the interpretation of experimental data on the NR operators entering  $a_{1,2}$ , i.e.,  $\mathcal{O}_{7,8,12,13,14}$  and  $\mathcal{O}_{17,21,22,23,25,26}$  for DM up to spin one. Furthermore, at the more fundamental level of relativistic field theory, several interesting DM scenarios are particularly affected by the sign of  $W_2$ . Especially, the interactions with electron or DM axial-vector or tensor currents can induce contributions related to  $W_2$ , and thus would be affected by the sign problem. The calculation details in this letter, together with the systematic constraints on other nonrelativistic and relativistic interactions from the latest experiments, will be provided in the accompanying long paper [33].

### Acknowledgements

This work was supported in part by the Guangdong Major Project of Basic and Applied Basic Research No.2020B0301030008, and by the Grants No.NSFC-12035008, No. NSFC-12247151, No. NSFC-12305110, and No. NSFC-12347121.

\* Electronic address: [jinhanliang@m.scnu.edu.cn](mailto:jinhanliang@m.scnu.edu.cn)

† Electronic address: [liaoy@m.scnu.edu.cn](mailto:liaoy@m.scnu.edu.cn)

‡ Electronic address: [maxid@scnu.edu.cn](mailto:maxid@scnu.edu.cn)

§ Electronic address: [whaolin@m.scnu.edu.cn](mailto:whaolin@m.scnu.edu.cn)

- [1] L. D. Duffy and K. van Bibber, “*Axions as Dark Matter Particles*,” *New J. Phys.* **11** (2009) 105008, [[arXiv:0904.3346](https://arxiv.org/abs/0904.3346)] [hep-ph].
- [2] M. Fabbrichesi, E. Gabrielli, and G. Lanfranchi, “*The Dark Photon*,” [[arXiv:2005.01515](https://arxiv.org/abs/2005.01515)] [hep-ph].
- [3] P. Agrawal *et al.*, “*Feebly-interacting particles: FIPs 2020 workshop report*,” *Eur. Phys. J. C* **81** no. 11, (2021) 1015, [[arXiv:2102.12143](https://arxiv.org/abs/2102.12143)] [hep-ph].
- [4] M. Drewes *et al.*, “*A White Paper on keV Sterile Neutrino Dark Matter*,” *JCAP* **01** (2017) 025, [[arXiv:1602.04816](https://arxiv.org/abs/1602.04816)] [hep-ph].
- [5] A. Boyarsky, M. Drewes, T. Lasserre, S. Mertens, and O. Ruchayskiy, “*Sterile neutrino Dark Matter*,” *Prog. Part. Nucl. Phys.* **104** (2019) 1–45, [[arXiv:1807.07938](https://arxiv.org/abs/1807.07938)] [hep-ph].
- [6] G. Arcadi, M. Dutra, P. Ghosh, M. Lindner, Y. Mambrini, M. Pierre, S. Profumo, and F. S. Queiroz, “*The waning of the WIMP? A review of models, searches, and constraints*,” *Eur. Phys. J. C* **78** no. 3, (2018) 203, [[arXiv:1703.07364](https://arxiv.org/abs/1703.07364)] [hep-ph].
- [7] L. Roszkowski, E. M. Sessolo, and S. Trojanowski, “*WIMP dark matter candidates and searches—current status and future prospects*,” *Rept. Prog. Phys.* **81** no. 6, (2018) 066201, [[arXiv:1707.06277](https://arxiv.org/abs/1707.06277)] [hep-ph].
- [8] PandaX-II Collaboration, X. Cui *et al.*, “*Dark Matter Results From 54-Ton-Day Exposure of PandaX-II Experiment*,” *Phys. Rev. Lett.* **119** no. 18, (2017) 181302, [[arXiv:1708.06917](https://arxiv.org/abs/1708.06917)] [astro-ph.CO].

- [9] **XENON** Collaboration, E. Aprile *et al.*, “First Dark Matter Search with Nuclear Recoils from the XENONnT Experiment,” *Phys. Rev. Lett.* **131** no. 4, (2023) 041003, [[arXiv:2303.14729](#) [hep-ex]].
- [10] **LZ** Collaboration, J. Aalbers *et al.*, “First Dark Matter Search Results from the LUX-ZEPLIN (LZ) Experiment,” *Phys. Rev. Lett.* **131** no. 4, (2023) 041002, [[arXiv:2207.03764](#) [hep-ex]].
- [11] **DarkSide** Collaboration, P. Agnes *et al.*, “Low-Mass Dark Matter Search with the DarkSide-50 Experiment,” *Phys. Rev. Lett.* **121** no. 8, (2018) 081307, [[arXiv:1802.06994](#) [astro-ph.HE]].
- [12] M. Schumann, “Direct Detection of WIMP Dark Matter: Concepts and Status,” *J. Phys. G* **46** no. 10, (2019) 103003, [[arXiv:1903.03026](#) [astro-ph.CO]].
- [13] C. Kouvaris and J. Pradler, “Probing sub-GeV Dark Matter with conventional detectors,” *Phys. Rev. Lett.* **118** no. 3, (2017) 031803, [[arXiv:1607.01789](#) [hep-ph]].
- [14] A. B. Migdal, “Ionization of atoms accompanying  $\alpha$ - and  $\beta$ -decay,” *J. Phys. A*, **449** (1941) (1941).
- [15] M. Ibe, W. Nakano, Y. Shoji, and K. Suzuki, “Migdal Effect in Dark Matter Direct Detection Experiments,” *JHEP* **03** (2018) 194, [[arXiv:1707.07258](#) [hep-ph]].
- [16] Y. Kahn and T. Lin, “Searches for light dark matter using condensed matter systems,” *Rept. Prog. Phys.* **85** no. 6, (2022) 066901, [[arXiv:2108.03239](#) [hep-ph]].
- [17] A. Mitridate, T. Trickle, Z. Zhang, and K. M. Zurek, “Snowmass white paper: Light dark matter direct detection at the interface with condensed matter physics,” *Phys. Dark Univ.* **40** (2023) 101221, [[arXiv:2203.07492](#) [hep-ph]].
- [18] **LZ** Collaboration, J. Aalbers *et al.*, “Search for new physics in low-energy electron recoils from the first LZ exposure,” *Phys. Rev. D* **108** no. 7, (2023) 072006, [[arXiv:2307.15753](#) [hep-ex]].
- [19] **XENON** Collaboration, E. Aprile *et al.*, “Light Dark Matter Search with Ionization Signals in XENON1T,” *Phys. Rev. Lett.* **123** no. 25, (2019) 251801, [[arXiv:1907.11485](#) [hep-ex]].
- [20] **XENON** Collaboration, E. Aprile *et al.*, “Emission of single and few electrons in XENON1T and limits on light dark matter,” *Phys. Rev. D* **106** no. 2, (2022) 022001, [[arXiv:2112.12116](#) [hep-ex]].
- [21] **XENON** Collaboration, E. Aprile *et al.*, “Search for New Physics in Electronic Recoil Data from XENONnT,” *Phys. Rev. Lett.* **129** no. 16, (2022) 161805, [[arXiv:2207.11330](#) [hep-ex]].
- [22] **PandaX** Collaboration, S. Li *et al.*, “Search for Light Dark Matter with Ionization Signals in the PandaX-4T Experiment,” *Phys. Rev. Lett.* **130** no. 26, (2023) 261001, [[arXiv:2212.10067](#) [hep-ex]].
- [23] **DarkSide** Collaboration, P. Agnes *et al.*, “Constraints on Sub-GeV Dark-Matter–Electron Scattering from the DarkSide-50 Experiment,” *Phys. Rev. Lett.* **121** no. 11, (2018) 111303, [[arXiv:1802.06998](#) [astro-ph.CO]].
- [24] **PandaX-II** Collaboration, C. Cheng *et al.*, “Search for Light Dark Matter-Electron Scatterings in the PandaX-II Experiment,” *Phys. Rev. Lett.* **126** no. 21, (2021) 211803, [[arXiv:2101.07479](#) [hep-ex]].
- [25] J. Kopp, V. Niros, T. Schwetz, and J. Zupan, “DAMA/LIBRA and leptonically interacting Dark Matter,” *Phys. Rev. D* **80** (2009) 083502, [[arXiv:0907.3159](#) [hep-ph]].
- [26] R. Essig, J. Mardon, and T. Volansky, “Direct Detection of Sub-GeV Dark Matter,” *Phys. Rev. D* **85** (2012) 076007, [[arXiv:1108.5383](#) [hep-ph]].
- [27] R. Essig, A. Manalaysay, J. Mardon, P. Sorensen, and T. Volansky, “First Direct Detection Limits on sub-GeV Dark Matter from XENON10,” *Phys. Rev. Lett.* **109** (2012) 021301, [[arXiv:1206.2644](#) [astro-ph.CO]].
- [28] B. M. Roberts, V. A. Dzuba, V. V. Flambaum, M. Pospelov, and Y. V. Stadnik, “Dark matter scattering on electrons: Accurate calculations of atomic excitations and implications for the DAMA signal,” *Phys. Rev. D* **93** no. 11, (2016) 115037, [[arXiv:1604.04559](#) [hep-ph]].
- [29] B. M. Roberts, V. V. Flambaum, and G. F. Gribakin, “Ionization of atoms by slow heavy particles, including dark matter,” *Phys. Rev. Lett.* **116** no. 2, (2016) 023201, [[arXiv:1509.09044](#) [physics.atom-ph]].
- [30] M. K. Pandey, L. Singh, C.-P. Wu, J.-W. Chen, H.-C. Chi, C.-C. Hsieh, C. P. Liu, and H. T. Wong, “Constraints from a many-body method on spin-independent dark matter scattering off electrons using data from germanium and xenon detectors,” *Phys. Rev. D* **102** no. 12, (2020) 123025, [[arXiv:1812.11759](#) [hep-ph]].
- [31] R. Catena, T. Emken, N. A. Spaldin, and W. Tarantino, “Atomic responses to general dark matter-electron interactions,” *Phys. Rev. Res.* **2** no. 3, (2020) 033195, [[arXiv:1912.08204](#) [hep-ph]].
- [32] R. Catena, D. Cole, T. Emken, M. Matas, N. Spaldin, W. Tarantino, and E. Urdshals, “Dark matter-electron interactions in materials beyond the dark photon model,” *JCAP* **03** (2023) 052, [[arXiv:2210.07305](#) [hep-ph]].
- [33] J.-H. Liang, Y. Liao, X.-D. Ma, and H.-L. Wang, “A systematic investigation on dark matter-electron scattering in effective field theories,” (In preparation).
- [34] R. Essig, M. Fernandez-Serra, J. Mardon, A. Soto, T. Volansky, and T.-T. Yu, “Direct Detection of sub-GeV Dark Matter with Semiconductor Targets,” *JHEP* **05** (2016) 046, [[arXiv:1509.01598](#) [hep-ph]].
- [35] B. M. Roberts and V. V. Flambaum, “Electron-interacting dark matter: Implications from DAMA/LIBRA-phase2 and prospects for liquid xenon detectors and NaI detectors,” *Phys. Rev. D* **100** no. 6, (2019) 063017, [[arXiv:1904.07127](#) [hep-ph]].
- [36] R. Essig, T. Volansky, and T.-T. Yu, “New Constraints and Prospects for sub-GeV Dark Matter Scattering off Electrons in Xenon,” *Phys. Rev. D* **96** no. 4, (2017) 043017, [[arXiv:1703.00910](#) [hep-ph]].
- [37] R. Essig, J. Pradler, M. Sholapurkar, and T.-T. Yu, “Relation between the Migdal Effect and Dark Matter-Electron Scattering in Isolated Atoms and Semiconductors,” *Phys. Rev. Lett.* **124** no. 2, (2020) 021801, [[arXiv:1908.10881](#) [hep-ph]].
- [38] X.-G. He, X.-D. Ma, and G. Valencia, “FCNC B and K meson decays with light bosonic Dark Matter,” *JHEP* **03** (2023) 037, [[arXiv:2209.05223](#) [hep-ph]].

| Operator  | Operator  | Operator   |
|---|---|--|
| $\mathcal{O}_1 = \mathbb{1}_x \mathbb{1}_e$   | $\mathcal{O}_{10} = \mathbb{1}_x \frac{i\mathbf{q}}{m_e} \cdot \mathbf{S}_e$  | $\mathcal{O}_{19} = \frac{\mathbf{q}}{m_e} \cdot \tilde{\mathbf{S}}_x \cdot \frac{\mathbf{q}}{m_e} \mathbb{1}_e$   |
| $\mathcal{O}_3 = \mathbb{1}_x \left( \frac{i\mathbf{q}}{m_e} \times \mathbf{v}_{\text{el}}^\perp \right) \cdot \mathbf{S}_e$      | $\mathcal{O}_{11} = \mathbf{S}_x \cdot \frac{i\mathbf{q}}{m_e} \mathbb{1}_e$  | $\mathcal{O}_{20} = -\frac{\mathbf{q}}{m_e} \cdot \tilde{\mathbf{S}}_x \cdot \left( \frac{\mathbf{q}}{m_e} \times \mathbf{S}_e \right)$  |
| $\mathcal{O}_4 = \mathbf{S}_x \cdot \mathbf{S}_e$   | $\mathcal{O}_{12} = -\mathbf{S}_x \cdot (\mathbf{v}_{\text{el}}^\perp \times \mathbf{S}_e)$   | $\mathcal{O}_{21} = \mathbf{v}_{\text{el}}^\perp \cdot \tilde{\mathbf{S}}_x \cdot \mathbf{S}_e$  |
| $\mathcal{O}_5 = \mathbf{S}_x \cdot \left( \frac{i\mathbf{q}}{m_e} \times \mathbf{v}_{\text{el}}^\perp \right) \mathbb{1}_e$      | $\mathcal{O}_{13} = (\mathbf{S}_x \cdot \mathbf{v}_{\text{el}}^\perp) \left( \frac{i\mathbf{q}}{m_e} \cdot \mathbf{S}_e \right)$                              | $\mathcal{O}_{22} = \left( \frac{i\mathbf{q}}{m_e} \times \mathbf{v}_{\text{el}}^\perp \right) \cdot \tilde{\mathbf{S}}_x \cdot \mathbf{S}_e + \mathbf{v}_{\text{el}}^\perp \cdot \tilde{\mathbf{S}}_x \cdot \left( \frac{i\mathbf{q}}{m_e} \times \mathbf{S}_e \right)$ |
| $\mathcal{O}_6 = \left( \mathbf{S} \cdot \frac{\mathbf{q}}{m_e} \right) \left( \frac{\mathbf{q}}{m_e} \cdot \mathbf{S}_e \right)$ | $\mathcal{O}_{14} = (\mathbf{S}_x \cdot \frac{i\mathbf{q}}{m_e}) (\mathbf{v}_{\text{el}}^\perp \cdot \mathbf{S}_e)$   | $\mathcal{O}_{23} = -\frac{i\mathbf{q}}{m_e} \cdot \tilde{\mathbf{S}}_x \cdot (\mathbf{v}_{\text{el}}^\perp \times \mathbf{S}_e)$  |
| $\mathcal{O}_7 = \mathbb{1}_x \mathbf{v}_{\text{el}}^\perp \cdot \mathbf{S}_e$  | $\mathcal{O}_{15} = \mathbf{S}_x \cdot \frac{\mathbf{q}}{m_e} \left[ \frac{\mathbf{q}}{m_e} \cdot (\mathbf{v}_{\text{el}}^\perp \times \mathbf{S}_e) \right]$ | $\mathcal{O}_{24} = \frac{\mathbf{q}}{m_e} \cdot \tilde{\mathbf{S}}_x \cdot \left( \frac{\mathbf{q}}{m_e} \times \mathbf{v}_{\text{el}}^\perp \right)$   |
| $\mathcal{O}_8 = \mathbf{S}_x \cdot \mathbf{v}_{\text{el}}^\perp \mathbb{1}_e$  | $\mathcal{O}_{17} = \frac{i\mathbf{q}}{m_e} \cdot \tilde{\mathbf{S}}_x \cdot \mathbf{v}_{\text{el}}^\perp \mathbb{1}_e$                                       | $\mathcal{O}_{25} = \left( \frac{\mathbf{q}}{m_e} \cdot \tilde{\mathbf{S}}_x \cdot \mathbf{v}_{\text{el}}^\perp \right) \left( \frac{\mathbf{q}}{m_e} \cdot \mathbf{S}_e \right)$  |
| $\mathcal{O}_9 = -\mathbf{S}_x \cdot \left( \frac{i\mathbf{q}}{m_e} \times \mathbf{S}_e \right)$                                  | $\mathcal{O}_{18} = \frac{i\mathbf{q}}{m_e} \cdot \tilde{\mathbf{S}}_x \cdot \mathbf{S}_e$  | $\mathcal{O}_{26} = \left( \frac{\mathbf{q}}{m_e} \cdot \tilde{\mathbf{S}}_x \cdot \frac{\mathbf{q}}{m_e} \right) (\mathbf{v}_{\text{el}}^\perp \cdot \mathbf{S}_e)$   |

TABLE I: The leading-order nonrelativistic DM-electron interactions. Here  $\mathbf{q} = \mathbf{p} - \mathbf{p}'$  with  $\mathbf{p}$  ( $\mathbf{p}'$ ) being the momentum of initial (final) DM state.  $\mathcal{O}_2$  and  $\mathcal{O}_{16}$  being quadratic in  $\mathbf{v}_{\text{el}}^\perp$  are not shown.

## Appendix

**Nonrelativistic operators for DM-electron scattering**—The NR DM-electron interactions can be built by using the identity and spin operators. For the electron (and fermion or vector DM), we denote the identity and spin operators by  $\mathbb{1}_e$  and  $\mathbf{S}_e$  ( $\mathbb{1}_x$  and  $\mathbf{S}_x$ ),  $x = \phi, \chi, X$  for the scalar, fermion, vector DM cases respectively. For the vector DM, besides  $\mathbb{1}_x$  and  $\mathbf{S}_x$ , a rank-two traceless spin tensor operator  $\tilde{\mathbf{S}}_x$  is needed:

$$\tilde{\mathbf{S}}_x^{ij} = \frac{1}{2} (S_x^i S_x^j + i \leftrightarrow j) - \frac{2}{3} \delta^{ij}. \quad (11)$$

Together with the momentum transfer  $\mathbf{q}$  and DM-electron transverse velocity  $\mathbf{v}_{\text{el}}^\perp$ , one can construct the relevant NR operators. In Table I, we summarize the most general NR operators for DM-electron scattering at leading order. The NR operator basis is given for operators that are at most quadratic in  $\mathbf{q}$  and linear in  $\mathbf{v}_{\text{el}}^\perp$  for a DM particle up to spin one. The operators from  $\mathcal{O}_1$  to  $\mathcal{O}_{15}$  were given previously in Refs. [31, 32], and the operators from  $\mathcal{O}_{17}$  to  $\mathcal{O}_{26}$  are specific to vector DM-electron scattering which can be generated by the relativistic interactions in [33, 38]. We note in passing that the basis of operators for DM-quark interactions can be obtained by changing the electron label to the flavor of quarks.

**Dark matter response functions**—The calculation details for DM response functions are given in the accompanying long paper [33]. For the DM up to spin one, the DM response functions are

- Scalar DM:

$$a_0 = c_1^2 + \frac{1}{4} c_{10}^2 x_e, \quad a_1 = \frac{1}{4} c_7^2 + \frac{1}{4} c_3^2 x_e, \quad a_2 = -\frac{1}{4} c_3^2 x_e. \quad (12)$$

- Fermion DM:

$$a_0 = c_1^2 + \frac{3}{16} c_4^2 + \left( \frac{1}{8} c_9^2 + \frac{1}{4} c_{10}^2 + \frac{1}{4} c_{11}^2 + \frac{1}{8} c_4 c_6 \right) x_e + \frac{1}{16} c_6^2 x_e^2, \quad (13a)$$

$$a_1 = \frac{1}{4} c_7^2 + \frac{1}{4} c_8^2 + \frac{1}{8} c_{12}^2 + \left( \frac{1}{4} c_3^2 + \frac{1}{4} c_5^2 + \frac{1}{16} c_{13}^2 + \frac{1}{16} c_{14}^2 - \frac{1}{8} c_{12} c_{15} \right) x_e + \frac{1}{16} c_{15}^2 x_e^2, \quad (13b)$$

$$a_2 = -\left( \frac{1}{4} c_3^2 + \frac{1}{4} c_5^2 - \frac{1}{8} c_{13} c_{14} - \frac{1}{8} c_{12} c_{15} \right) x_e - \frac{1}{16} c_{15}^2 x_e^2. \quad (13c)$$

- Vector DM:

$$a_0 = c_1^2 + \frac{1}{2} c_4^2 + \left( \frac{1}{3} c_9^2 + \frac{1}{4} c_{10}^2 + \frac{2}{3} c_{11}^2 + \frac{5}{36} c_{18}^2 + \frac{1}{3} c_4 c_6 \right) x_e + \left( \frac{1}{6} c_6^2 + \frac{2}{9} c_{19}^2 + \frac{1}{12} c_{20}^2 \right) x_e^2, \quad (14a)$$

$$a_1 = \frac{1}{4} c_7^2 + \frac{2}{3} c_8^2 + \frac{1}{3} c_{12}^2 + \frac{5}{36} c_{21}^2 + \left( \frac{1}{4} c_3^2 + \frac{2}{3} c_5^2 + \frac{1}{6} c_{13}^2 + \frac{1}{6} c_{14}^2 + \frac{1}{6} c_{17}^2 + \frac{3}{8} c_{22}^2 + \frac{7}{72} c_{23}^2 - \frac{1}{3} c_{12} c_{15} \right. \\ \left. + \frac{1}{12} c_{22} c_{23} + \frac{1}{12} c_{21} c_{25} - \frac{1}{18} c_{21} c_{26} \right) x_e + \left( \frac{1}{6} c_{15}^2 + \frac{1}{6} c_{24}^2 + \frac{1}{24} c_{25}^2 + \frac{1}{18} c_{26}^2 \right) x_e^2, \quad (14b)$$

$$\begin{aligned}
a_2 = & - \left( \frac{1}{4}c_3^2 + \frac{2}{3}c_5^2 - \frac{1}{18}c_{17}^2 + \frac{7}{24}c_{22}^2 + \frac{1}{72}c_{23}^2 - \frac{1}{3}c_{13}c_{14} - \frac{1}{3}c_{12}c_{15} - \frac{1}{36}c_{21}c_{25} - \frac{1}{6}c_{21}c_{26} + \frac{1}{4}c_{22}c_{23} \right) x_e \\
& - \left( \frac{1}{6}c_{15}^2 + \frac{1}{6}c_{24}^2 - \frac{1}{72}c_{25}^2 - \frac{1}{9}c_{25}c_{26} \right) x_e^2.
\end{aligned} \tag{14c}$$

In the above, we highlight the dependence on  $x_e = \mathbf{q}^2/m_e^2$  in cyan that helps to identify the NR operators with leading order contributions. The above results are for the case of real WCs  $c_i$  that correspond to Hermitian operators for the elastic DM scenario. For the complex WCs, the results are obtained by changing  $c_i c_j \rightarrow \text{Re}(c_i^* c_j)$  in each term. The case with complex WCs could appear in the inelastic DM scenario, all of which will be provided in [33].

**Atomic response functions**—The definition for the atomic response functions  $W_{1,2,3,4}$  is as follows [31],

$$W_1 = V \frac{4k'^3}{(2\pi)^3} \sum_{m=-\ell}^{\ell} \sum_{\ell'=0}^{\infty} \sum_{m'=-\ell'}^{\ell'} |f_{1 \rightarrow 2}(\mathbf{q})|^2, \tag{15a}$$

$$W_2 = V \frac{4k'^3}{(2\pi)^3} \sum_{m=-\ell}^{\ell} \sum_{\ell'=0}^{\infty} \sum_{m'=-\ell'}^{\ell'} \frac{\mathbf{q}}{m_e} \cdot f_{1 \rightarrow 2}(\mathbf{q}) f_{1 \rightarrow 2}^*(\mathbf{q}), \tag{15b}$$

$$W_3 = V \frac{4k'^3}{(2\pi)^3} \sum_{m=-\ell}^{\ell} \sum_{\ell'=0}^{\infty} \sum_{m'=-\ell'}^{\ell'} |\mathbf{f}_{1 \rightarrow 2}(\mathbf{q})|^2, \tag{15c}$$

$$W_4 = V \frac{4k'^3}{(2\pi)^3} \sum_{m=-\ell}^{\ell} \sum_{\ell'=0}^{\infty} \sum_{m'=-\ell'}^{\ell'} \left| \frac{\mathbf{q}}{m_e} \cdot \mathbf{f}_{1 \rightarrow 2}(\mathbf{q}) \right|^2. \tag{15d}$$

Here the summations have been performed over the magnetic quantum number ( $m$ ) for the initial electron state and the angular and magnetic quantum numbers ( $\ell'$  and  $m'$ ) for the final electron state, and  $V$  is the normalization volume. Notice the definition of  $W_{1,2,3,4}$  are independent of specific DM properties. Although the three new combinations of atomic response functions ( $\widetilde{W}_{0,1,2}$ ) are related to the DM mass through  $y_e$ , we emphasize that they are useful for understanding which NR operators give dominant contributions, as discussed in the paper.